Available online at http://ijcpe.uobaghdad.edu.iq and www.iasj.net
Iraqi Journal of Chemical and Petroleum Engineering
Vol.23 No.3 (September 2022) 1 – 9
EISSN: 2618-0707, PISSN: 1997-4884

Mathematical Modeling of a Hollow Fiber Module Used in Pressure-Retarded Osmosis Process

Farah Adil Yaseen [a], Ahmed Faiq Al-Alawy [b], Adel Sharif [c]

[a] *Iraq National Oil Company, Midland Oil Company, Baghdad, Iraq*
[b] *Department of Chemical Engineering, College of Engineering, University of Baghdad, Baghdad, Iraq*
[c] *Department of Chemical and Process Engineering, University of Surrey, Surrey, UK*

Abstract

Pressure retarded osmosis (PRO) can be considered as one of the methods for utilizing osmotic power, which is a membrane-based technology. Mathematical modeling plays an essential part in the development and optimization of PRO energy-generating systems. In this research, a mathematical model was developed for the hollow fiber module to predict the power density and the permeate water flux theoretically. Sodium chloride solution was employed as the feed and draw solution. Different operating parameters, draw solution concentration (1 and 2 M), the flow rate of draw solution (2, 3, and 4 L/min), and applied hydraulic pressure difference (0 - 90 bar) was used to evaluate the performance of PRO process of a hollow fiber module. The effect of these operational parameters was investigated on the theoretical permeate water flux and power density. According to the theoretical results, the permeate water flux and the power density increased with increasing the concentration of draw solution and the flow rate of the draw solution. While decreased with increasing the feed solution concentration. By increasing the applied hydraulic pressure on the draw solution, the water flux decreased and the produced power density increased. The maximum power density and the corresponding permeate water flux of 2 M NaCl draw solution was approximately 16.414 W/m^2 and 11.818 LMH respectively, which occurs at an applied hydraulic pressure of 50 bar.

Keywords: Mathematical model, Osmotic Power, Hollow Fiber Membrane, Pressure Retarded Osmosis.

Received on 17/05/2022, Accepted on 04/06/2022, published on 30/09/2022

https://doi.org/10.31699/IJCPE.2022.3.1

1- Introduction

Pressure retarded osmosis (PRO) can be considered as one of the methods for utilizing osmotic power, which is a membrane-based technology [1]. It is considered as one of the renewable energies, which was investigated over the last decade intensively [2] due to its superior energy efficiency and high power density, as well as its compatibility with highly salty solutions [3]. The energy-releasing process through the mixing of salt-water and fresh-water can be demonstrated by considering basic osmotic principles [4]. The process of PRO can be considered as one of the most widely investigated technologies for harnessing salinity gradients and converting the osmotic power into useful work [5]. The pressure retarded osmosis process utilizes the osmotic pressure difference that develops when a semipermeable membrane separates two different concentration solutions for driving the water permeation from the low-concentration solution "feed solution FS" into the high-concentration solution "draw solution DS". A hydraulic pressure less than the osmotic pressure difference is applied to the draw solution, thereby "retarding" the flux of water across the semipermeable membrane. A hydro-turbine extracts useful work from the expanding volume of the draw solution [6].

It is considered as an intermediate between reverse osmosis (RO) and forward osmosis (FO) processes. The same as to RO, the hydraulic pressure is applied to the side of the draw solution against the osmotic pressure gradient but it is smaller than the osmotic pressure difference. Consequently the net flux of water remains towards the concentrated draw solution, which is in a direction identical to that of the FO process [7]. Fig. **1** represents the flux directions and driving force for the PRO process that is occurring because of the contact of pure water and saline water through a semipermeable membrane [8].

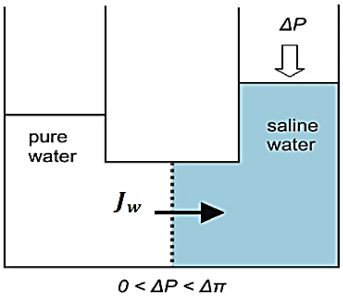

Fig. 1. Representation of Solvent Flow in Pressure Retarded Osmosis (PRO) [8]

Corresponding Authors: Name: Farah Adil Yaseen , Email: phdfarah88@yahoo.com , Name: Ahmed Faiq Al-Alawy, Email: Ahmedalalawy@yahoo.com, : Name: Adel Sharif , Email: a.sharif@surrey.ac.uk

In 2009, Statkraft, which is a Norwegian company in the clean energy sector, has constructed the first prototype plant of osmotic power in the world by mixing seawater and fresh river water across a semi-permeable membrane. It is planning to commercialize osmotic power with a projected energy cost-competitive against other renewable energy sources.

Based on Statkraft, the power density of the membrane was determined to be between 4 - 6 W/m^2 to make PRO profitable [9]. Another prototype hybrid RO-PRO was constructed by the Mega-ton Water System project in Japan in 2010. This plant aimed to hybridize seawater reverse osmosis (SWRO) and wastewater reclamation systems for power generation. The maximal power density of this system was 13.3 W/m^2 at about 27 bar hydraulic pressure difference [10], [11].

Yasukawa et al., 2018 [12] had examined the efficiency of pressure-retarded osmosis process using CTA hollow-fiber membrane, the maximum power density was 0.14 W/m^2 at about 4 bar hydraulic pressure difference when using 0.5 M NaCl as draw solution DS and Tap water as feed solution.

The research aims to develop a mathematical model of the water flux and power density for a PRO hollow fiber membrane and examine the effect of many parameters on the performance of the pressure retarded osmosis process theoretically.

2- Modeling

The mathematical model describes the mass transport in detail in four transport-zones, which are boundary layers on the two surfaces of the membrane, within the porous-support layer, and across the active layer of the membrane. The precise mass transport description is highly significant for the evaluation of the performance of the HF membrane. Therefore, the mathematical model was developed by using the minimum of assumptions, so it takes into consideration all negative effects that reduce the performance of the PRO process.

2.1. Mass Transport in the Realistic Hollow Fiber Membrane

Fig. **2** illustrates a cross-section of a hollow fiber membrane with an active layer at the outer HF surface. The draw solution is in direct contact with the active layer outside the hollow fiber, whereas the feed solution is inside the hollow fiber.

In this type of configuration, water radially permeates, through porous-support and active layers, toward the DS outside hollow fiber (shell-side). On the contrary, the solute diffuses down the concentration gradient from DS outside to feed solution within hollow fiber (lumen-side).

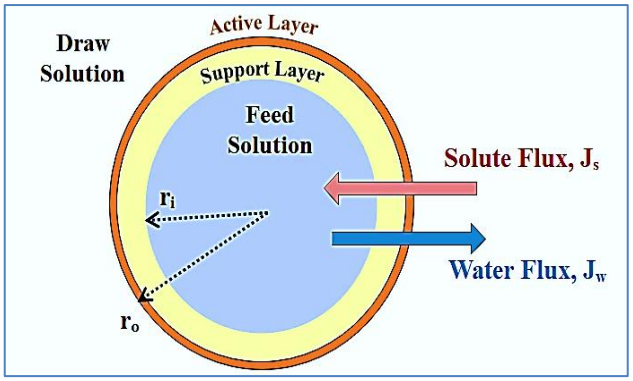

Fig. 2. Schematic Showing the Cross-Section of HF Membrane and its Geometrical Parameters

With a realistic membrane and hydrodynamics, four phenomena are occurring that reduce the trans-membrane water flux and power generation in the PRO process as presented in Fig. **3**:

1. The concentrative external concentration polarization ($ECP_{concentrative}$) on the feed solution side raises $C_{F,b}$ (bulk feed solution concentration) to $C_{F,m}$ (solute concentration on the support layer of membrane surface that faces feed solution).
2. The dilutive external concentration polarization ($ECP_{dilutive}$) on the draw side reduces $C_{D,b}$ (bulk draw solution concentration) to $C_{D,m}$ (solute concentration on the active layer of the membrane surface that faces draw solution).
3. The internal concentration polarization (ICP) within the porous support layer elevates the solute concentration from $C_{F,m}$ to $C_{F,i}$ (solute-concentration at the interface between the active layer and the support layer).
4. The reverse salt ions diffuse from the draw solution to the feed solution because of the concentration gradient across the membrane.

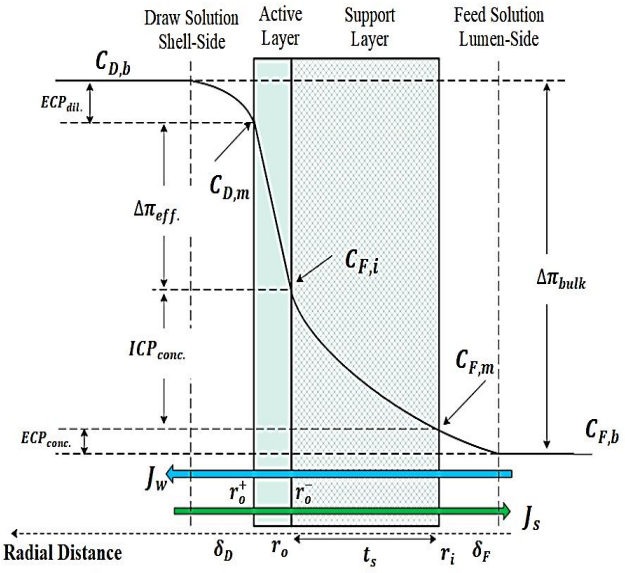

Fig. 3. Concentration Profile Over an HF Membrane

As illustrated in Fig. **3**, the effects of both ECP and ICP combine to reduce the osmotic pressure difference across the membrane to some effective value $\Delta\pi_{eff.}$ that is much smaller than $\Delta\pi$.

a. Mass Transport in Support and Boundary Layers

The salt mass transport in the porous-support layer of membrane and the boundary layer for each membrane side will equal the summation of diffusive and convective salt transport. The diffusive salt transport is defined by Fick's law, whereas the convective transport of salt represents the product of the local solute concentration $C(r)$ and the water flux $J_w(r)$. Hence, the salt mass transfer can be expressed by the general equation at the radial position (r) [13]:

$$J_s(r) = D' \frac{dC(r)}{dr} - J_w(r).C(r) \quad (1)$$

Where: $J_w(r)$ represents the water flux, $J_s(r)$ represents the salt flux, $C(r)$ represents the concentration of the salt at the radial position r, and D' represents the solute general diffusion coefficient.

The fluxes $J_w(r)$ and $J_s(r)$ in Eq. (1) are the areal fluxes that represent volume flow rate across a unit area of the membrane. The fluxes are not constant with respect to r due to the available area of flow changes in the radial direction. However, the linear fluxes that represent the volume flow rate through a unit length of the hollow fiber membrane, are constant and independent of the radial-position. Thus, Eq. (1) can be re-written by converting the areal water flux $J_w(r)$ and areal solute flux $J_s(r)$ to linear water flux ξ_w and linear solute flux ξ_s, respectively, $\xi_w = 2\pi r J_w(r)$ and $\xi_s = 2\pi r J_s(r)$:

$$\xi_s = 2\pi r D' \frac{dC(r)}{dr} - \xi_w.C(r) \quad (2)$$

Dividing Eq. (2) by ξ_w gives:

$$\frac{\xi_s}{\xi_w} = \frac{2\pi r D'}{\xi_w}\frac{dC(r)}{dr} - C(r) \quad (3)$$

Eq. (3) can be solved as an ordinary differential equation by applying the separation of variables method. Rearrangement of Eq. (3) to separate the variables:

$$\frac{dr}{r} = \frac{2\pi D'}{\xi_w}\frac{dC(r)}{C(r)+\frac{\xi_s}{\xi_w}} \quad (4)$$

- Porous Support Layer

In the porous-support layer of the membrane, the differential equation (Eq. 4) can be used, but, the general diffusion coefficient (D') simply represents the effective solute diffusion coefficient in the porous-support layer (D_s):

$$\frac{dr}{r} = \frac{2\pi D_s}{\xi_w}\frac{dC(r)}{C(r)+\frac{\xi_s}{\xi_w}} \quad (5)$$

The solute diffusion coefficient in the porous-support layer D_s is given by [14]:

$$D_s = \frac{D_F.\varepsilon}{\tau} \quad (6)$$

Where: D_F is the solute diffusion coefficient in the bulk feed solution, ε , and τ are the porosity and the tortuosity of the support layer structure of the membrane. Therefore, Eq. (5) can be rewritten as:

$$\frac{dr}{r} = \frac{2\pi\frac{D_F.\varepsilon}{\tau}}{\xi_w}\frac{dC(r)}{C(r)+\frac{\xi_s}{\xi_w}} \quad (7)$$

The thickness of the active layer is very small in comparison with the thickness of the porous support layer and the boundary layers. Therefore, no differentiation is done between the positions on both sides of the active layer when formulating the boundary conditions (i.e., $r_o^+ = r_o^- = r_o$) (Fig. 3) [15].

$$C(r = r_i) = C_{F,m} \quad \text{B.C.1}$$

$$C(r = r_o^- = r_o) = C_{F,i} \quad \text{B.C.2}$$

Integration over the porous membrane structure with the B.C. 1 and 2 yields:

$$\int_{r_o}^{r_i}\frac{dr}{r} = \frac{2\pi\frac{D_F.\varepsilon}{\tau}}{\xi_w}\int_{C_{F,i}}^{C_{F,m}}\frac{dC(r)}{C(r)+\frac{\xi_s}{\xi_w}} \quad (8)$$

giving the solution:

$$\ln\left(\frac{r_i}{r_o}\right) = \frac{2\pi\frac{D_F.\varepsilon}{\tau}}{\xi_w}\ln\left(\frac{C_{F,m}+\frac{\xi_s}{\xi_w}}{C_{F,i}+\frac{\xi_s}{\xi_w}}\right) \quad (9)$$

which can also be rewritten as Eq. (10):

$$C_{F,i} = \left(C_{F,m} + \frac{\xi_s}{\xi_w}\right)\left(\frac{r_o}{r_i}\right)^{\frac{\xi_w.\tau}{2\pi D_F.\varepsilon}} - \frac{\xi_s}{\xi_w} \quad (10)$$

- Draw Solution Boundary Layer

On the draw solution side, solutes are diluted at the surface as water enters from the feed side, giving rise to dilutive ECP. As a result, the effective osmotic pressure difference would reduce from $\pi_{D,b}$ to $\pi_{D,m}$.

The reverse draw solute flux on the side of the draw solution can also be derived using the same differential equation as in Eq. (4), with different boundary conditions. Thus, the boundary conditions for ECP on the draw solution side are:

$$C(r = r_o^+ = r_o) = C_{D,m} \quad \text{B.C.3}$$

$$C(r = r_o + \delta_D) = C_{D,b} \quad \text{B.C.4}$$

Where: δ_D represents the thickness of the DS boundary layer. Eq. (4) can be integrated over the draw solution boundary layer with B.C. 3 and 4. Here, the general diffusion coefficient (D') represents the solute diffusion coefficient in the bulk draw solution (D_D).

$$\int_{r_o}^{r_o+\delta_D} \frac{dr}{r} = \frac{2\pi D_D}{\xi_w} \int_{C_{D,m}}^{C_{D,b}} \frac{dC(r)}{C(r)+\frac{\xi_s}{\xi_w}} \quad (11)$$

giving the solution:

$$\ln\left(\frac{r_o+\delta_D}{r_o}\right) = \frac{2\pi D_D}{\xi_w} \ln\left(\frac{C_{D,b}+\frac{\xi_s}{\xi_w}}{C_{D,m}+\frac{\xi_s}{\xi_w}}\right) \quad (12)$$

Which: can also be rewritten as Eq. (13):

$$C_{D,m} = \left(C_{D,b} + \frac{\xi_s}{\xi_w}\right)\left(\frac{r_o}{r_o+\delta_D}\right)^{\frac{\xi_w}{2\pi D_D}} - \frac{\xi_s}{\xi_w} \quad (13)$$

- Film Thickness on the Draw Solution Side

The film thickness on the draw solution side of the membrane δ_D (shell side) is given by [16]:
where k_D represents the mass transfer coefficient for the draw solution, can be defined by [17]:

$$\delta_D = \frac{D_D}{k_D} \quad (14)$$

$$k_D = \frac{Sh_s.D_D}{d_h} \quad (15)$$

Where: Sh_s is the Sherwood number at the shell side, and d_h is the hydraulic diameter at the shell side of the membrane. The Sherwood number is determined from the following correlations [18]:

$$Sh_s = 1.25\, Sc_s^{1/3}\left(Re_s \frac{d_h}{L}\right)^{0.93} \quad (Re = 0 - 500) \quad (16)$$

Where: L is the module length, Sc_s and Re_s are the Schmidt and Reynolds numbers at the shell side, respectively. The Reynold and Schmidt numbers are determined as:

$$Re_s = \frac{\rho_D.u_D.d_h}{\mu_D} \quad (17)$$

$$Sc_s = \frac{\mu_D}{\rho_D.D_D} \quad (18)$$

Where: ρ_D and μ_D are the density and dynamic viscosity of the draw solution, respectively, and u_D is the velocity of the draw solution in the shell side and can be calculated as:

$$u_D = \frac{Q_D}{A_s} \quad (19)$$

Where: Q_D represents the volumetric flow rate of draw solution in the shell side, and A_s is the cross-sectional area of the shell side and can be calculated as:

$$A_s = \frac{\pi}{4}\left(D_{i,module}^2 - N_{fiber} d_o^2\right) \quad (20)$$

Where: N_{fiber} is the number of fibers in the module, $D_{i,module}$ represents the inner diameter of the module, d_o is the outer diameter of the fiber.
The hydraulic diameter of the shell side can be determined as [19]:

- Feed Solution Boundary Layer

A similar derivation can be conducted at the feed solution side with B.C. 5 and 6. Here, the general diffusion coefficient (D') represents the solute diffusion coefficient in the bulk feed solution (D_F).

$$C(r = r_i - \delta_F) = C_{F,b} \quad \text{B.C.5}$$

$$C(r = r_i) = C_{F,m} \quad \text{B.C.6}$$

Where: δ_F represents the thickness of the FS boundary layer.

$$\int_{r_i}^{r_i-\delta_F} \frac{dr}{r} = \frac{2\pi D_F}{\xi_w} \int_{C_{F,m}}^{C_{F,b}} \frac{dC(r)}{C(r)+\frac{\xi_s}{\xi_w}} \quad (22)$$

Giving the solution:

$$C_{F,m} = \left(C_{F,b} + \frac{\xi_s}{\xi_w}\right)\left(\frac{r_i}{r_i-\delta_F}\right)^{\frac{\xi_w}{2\pi D_F}} - \frac{\xi_s}{\xi_w} \quad (23)$$

Substituting Eq. (23) for $C_{F,m}$ in Eq. (10) gives an expression for the concentration at the active layer-support layer interface, $C_{F,i}$, that only depends on the bulk concentration.

$$C_{F,i} = \left(\left(C_{F,b} + \frac{\xi_s}{\xi_w}\right)\left(\frac{r_i}{r_i-\delta_F}\right)^{\frac{\xi_w}{2\pi D_F}}\right)\left(\frac{r_o}{r_i}\right)^{\frac{\xi_w.\tau}{2\pi D_F.\varepsilon}} - \frac{\xi_s}{\xi_w} \quad (24)$$

- Film Thickness on the Feed Solution Side

The film thickness on the feed solution side of the membrane δ_F (Lumen-Side) is given by [16]:

$$\delta_F = \frac{D_F}{k_F} \quad (25)$$

Where k_F represents the mass transfer coefficient for the feed solution, and can be defined by [20]:

$$k_F = \frac{Sh_l.D_F}{d_i} \quad (26)$$

d_i represents the inner diameter of the HF membrane, and Sh_l is the Sherwood number at the lumen side, which is determined from the following correlations [21]:

$$Sh_l = 1.62\ Sc_l^{1/3}.Re_l^{1/3}\left(\frac{d_i}{L}\right)^{1/3} = 1.62\ Gz_l^{1/3},\ Gz_l \geq 6 \quad (27)$$

Or

$$Sh_l = 0.5\ Sc_l.Re_l\left(\frac{d_i}{L}\right) = 0.5\ Gz_l\ , \qquad Gz_l < 6 \quad (28)$$

Where: L is the module length, Sc_l and Re_l are the Schmidt and Reynolds numbers at the lumen side, respectively. Gz_l is the Graetz number at the lumen side, defined as $Re_l\ .Sc_l.d_i/L$. The Reynold and Schmidt numbers are calculated as follows:

$$Re_l = \frac{\rho_F.u_F.d_i}{\mu_F} \quad (29)$$

$$Sc_l = \frac{\mu_F}{\rho_F.D_F} \quad (30)$$

Where: u_F is the velocity of the feed solution in the lumen side, d_i is the inner diameter of the fiber, ρ_F, and μ_F are the density and dynamic viscosity of the feed solution, respectively.

$$u_F = \frac{Q_F}{A_l} \quad (31)$$

Where: Q_F represents the volumetric flow rate of feed solution in the lumen side, and A_l is the cross-sectional area of the lumen side and can be calculated as follows:

$$A_l = N_{fiber}\ \frac{\pi}{4}\ d_i^2 \quad (32)$$

b. Mass Transport across Active Layer

The mass transport equations related to the water flux and solute flux through the active layer membrane at position r_o are described by [15]:

$$J_w(r_o) = \frac{\xi_w}{2\pi r_o} = A(\Delta\pi_{active} - \Delta P) \quad (33)$$

The effective osmotic pressure, $\Delta\pi_{active}$, that governs the mechanism is [22], [23]:

$$\Delta\pi_{active} = (\pi_{D,m} - \pi_{F,i}) \quad (34)$$

Therefore, Eq. (33) can be written as:

$$J_w(r_o) = \frac{\xi_w}{2\pi r_o} = A(\pi_{D,m} - \pi_{F,i} - \Delta P) \quad (35)$$

and the salt flux through the active layer is written as:

$$J_s(r_o) = \frac{\xi_s}{2\pi r_o} = B(C_{D,m} - C_{F,i}) \quad (36)$$

Where: B represents the salt permeability coefficient. The osmotic pressure (π) of any solution can be defined using Van't Hoff's equation [24], [25]:

$$\pi = nCR_gT \quad (37)$$

Where: n is the number of ions in the dissociated salt, C is the solute molar concentration, R_g represents the gas constant, and T represents the temperature of the solution. Thus, we consider that:

$$\pi_{D,m} = nR_gTC_{D,m} \quad (38)$$

$$\pi_{F,i} = nR_gTC_{F,i} \quad (39)$$

$$\pi_{F,m} = nR_gTC_{F,m} \quad (40)$$

Therefore, Eq. (35) for the water flux can be rewritten as: Dividing Eq. (36) by Eq. (41) yields the specific salt flux in PRO, as follows:

$$J_w(r_o) = \frac{\xi_w}{2\pi r_o} = AnR_gT(C_{D,m} - C_{F,i}) - A\Delta P \quad (41)$$

$$\frac{\xi_s}{\xi_w} = \frac{B}{AnR_gT}\left(1 + \frac{A\Delta P}{\xi_w/2\pi r_o}\right) \quad (42)$$

Substituting $C_{D,m}$ in Eq. (41) with its expression presented in Eq. (13) and substituting ξ_s/ξ_w with its expression developed in Eq. (42) yields Eq. (43):

$$\pi_{D,m} = \left(\pi_{D,b} + \frac{B}{A}\left(1 + \frac{A\Delta P}{\xi_w/2\pi r_o}\right)\right)\left(\frac{r_o}{r_o+\delta_D}\right)^{\frac{\xi_w}{2\pi D_D}} - \frac{B}{A}\left(1 + \frac{A\Delta P}{\xi_w/2\pi r_o}\right) \quad (43)$$

Substituting $C_{F,i}$ in Eq. (41) with its expression presented in Eq. (24) and substituting ξ_s/ξ_w with its expression developed in Eq. (42) yields Eq. (44):

$$\pi_{F,i} = \left(\pi_{F,b} + \frac{B}{A}\left(1 + \frac{A\Delta P}{\xi_w/2\pi r_o}\right)\right)\left(\frac{r_i}{r_i-\delta_F}\right)^{\frac{\xi_w}{2\pi D_F}}\left(\frac{r_o}{r_i}\right)^{\frac{\xi_w.\tau}{2\pi\ D_F.\varepsilon}} - \frac{B}{A}\left(1 + \frac{A\Delta P}{\xi_w/2\pi r_o}\right) \quad (44)$$

Substituting $\pi_{D,m}$ and $\pi_{F,i}$ in Eq. (35) with its expression presented in Eq. (43) and Eq. (44) respectively, yields Eq. (45):

$$\xi_w = 2\pi r_o A\left[\left(\pi_{D,b} + \frac{B}{A}\left(1 + \frac{A\Delta P}{\xi_w/2\pi r_o}\right)\right)\left(\frac{r_o}{r_o+\delta_D}\right)^{\frac{\xi_w}{2\pi D_D}} - \left(\pi_{F,b} + \frac{B}{A}\left(1 + \frac{A\Delta P}{\xi_w/2\pi r_o}\right)\right)\left(\frac{r_i}{r_i-\delta_F}\right)^{\frac{\xi_w}{2\pi D_F}}\left(\frac{r_o}{r_i}\right)^{\frac{\xi_w.\tau}{2\pi\ D_F.\varepsilon}} - \Delta P\right] \quad (45)$$

Replacing the linear flux, ξ_w, in Eq. (45) with the areal flux, J_w, by noting that $\xi_w = 2\pi r_o\ J_w$:

$$J_w = A\left[\left(\pi_{D,b} + \frac{B}{A}\left(1 + \frac{A\Delta P}{J_w}\right)\right)\left(\frac{r_o}{r_o+\delta_D}\right)^{\frac{r_o J_w}{D_D}} - \left(\pi_{F,b} + \frac{B}{A}\left(1 + \frac{A\Delta P}{J_w}\right)\right)\left(\frac{r_i}{r_i-\delta_F}\right)^{\frac{r_o J_w}{D_F}}\left(\frac{r_o}{r_i}\right)^{\frac{r_o J_w \cdot \tau}{D_F \cdot \varepsilon}} - \Delta P\right] \quad (46)$$

The terms in equations 46 and 47 are membrane parameters, solution properties, and measurable system conditions. The mathematical model for the PRO process was solved iteratively by the aid of the Microsoft Excel Program 2010 for a range of operating conditions to determine the permeate water flux.

The water flux equation, Eq. 46 was solved using Goal Seek Function by providing an initial guess and then updating iteratively. According to the study, the hollow fibre PRO membrane has water permeability coefficient equal to 0.471 L/m2 h.bar, salt permeability coefficient equal to 0.384 L/m2 h, and structural parameter equal to 855µm.

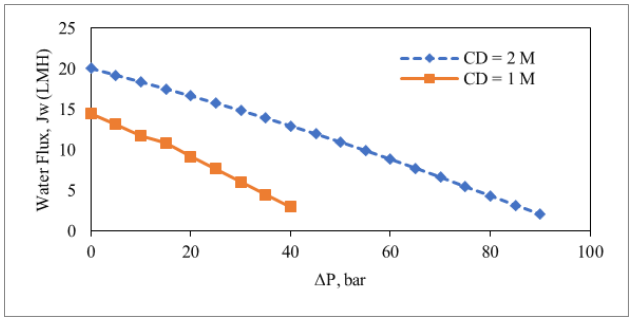

Fig. 4. Modeled Water Flux Vs. Applied Pressure Difference for Different DS Concentrations (FS = 0.25 g/L NaCl, T = 35 ºC, Q_D = 2 L/min, Q_F = 1 L/min)

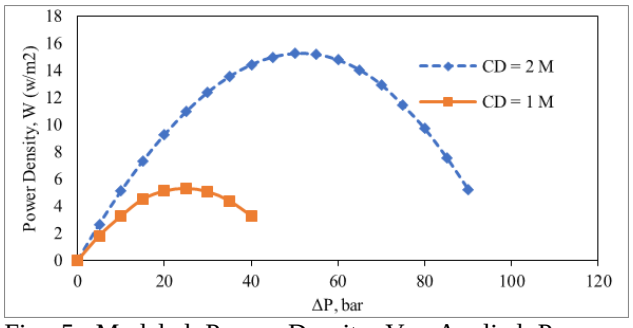

Fig. 5. Modeled Power Density Vs. Applied Pressure Difference for Different DS Concentrations (FS = 0.25 g/L NaCl, T = 35 ºC, Q_D = 2 L/min, Q_F = 0.1 L/min)

Fig. **6** and Fig. **7** demonstrate the impacts of applied pressure difference on the water flux and power density of the PRO system under various feed solution concentrations. The other conditions such as temperature (35 ℃), DS flow rate (2 L/min), FS flow rate (1 L/min) were kept constant. As expected, the water flux and power density values decrease as the feed solution concentration becomes higher. Increasing the feed solution concentration from 0.25 g/L (Tap Water) to 10 g/L (High-Salinity brackish water) led to a decrease in both water flux (Fig. **6**) and power density (Fig. **7**).

Increasing the concentration of the feed solution induces a reduction in the effective osmotic pressure difference; hence, the driving force of the PRO process decreases. When the feed solution concentration was increased from 0.25 g/L to 10 g/L, the power density decreased about 85% as shown in Figure 7.

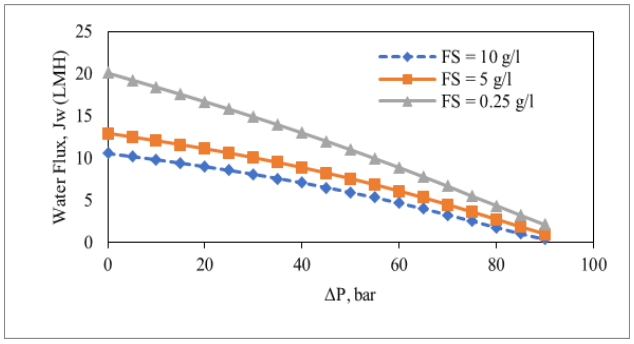

Fig. 6. Modeled Water Flux Vs. Applied Pressure Difference for Different FS Concentrations (DS = 2M NaCl, T = 35 ºC, Q_D = 2 L/min, Q_F = 1 L/min)

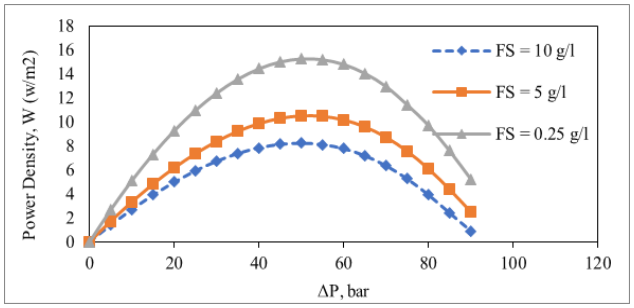

Fig. 7. Modeled Power Density Vs. Applied Pressure Difference for Different FS Concentrations (DS = 2M NaCl, T = 35 ºC, Q_D = 2 L/min, Q_F = 1 L/min)

Fig. **8** and Fig. **9** represent the impact of the DS flow rate on the PRO performance. They show how the water flux and and power density varies with hydraulic difference for various flow rates of draw solution (2, 3 and 4 L/min).

As the DS flow rate increased, there was a little increase in the water flux and power density, such an increase was because of the decrease in the DS dilution effect.

Also, the flow changes the mass transfer boundary layer thickness at the membrane surface.

It was observed that the power density increased around only 8 % when the flow rate of the draw solution was increased from 2 L/min to 4 L/min at 50 bar applied pressure difference.

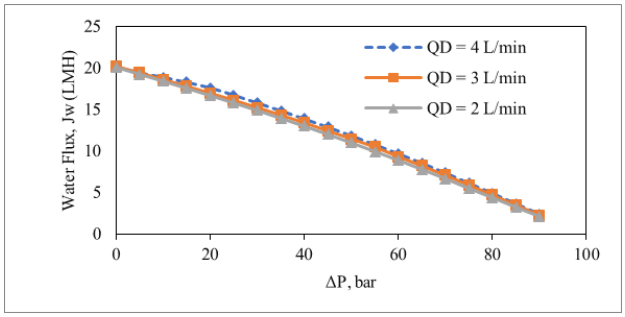

Fig. 8. Modeled Water Flux vs. Applied Pressure Difference for Different Flow Rates of Draw Solution (FS = 0.25 g/l, DS = 2M NaCl, T = 35 ºC, Q_F = 0.1 L/min)

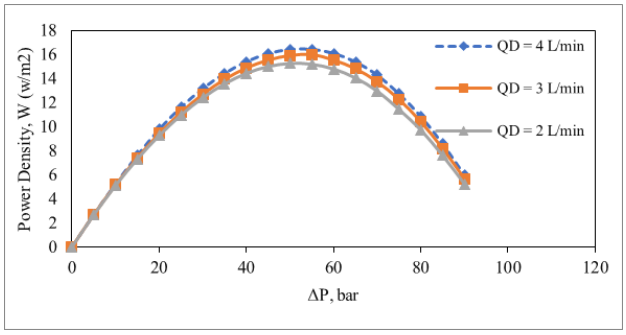

Fig. 9. Modeled Power Density Vs. Applied Pressure Difference for Different Flow Rates of Draw Solution (FS = 0.25 g/l, DS = 2M NaCl, T = 35 ºC, Q_F = 0.1 L/min)

4- Conclusion

In this study, a mathematical model was developed for the HF module to predict J_w and W theoretically by using the minimum of assumptions, so it takes into consideration all negative effects that reduce the performance of the PRO process. Maximum power density (15.248 W/m^2) occurred at an applied pressure difference of 50 bar for 2M draw solution concentration (102.8 bar osmotic pressure).

Therefore, this means that the maximum power density has occurred at an applied pressure difference of around 50% of the osmotic pressure difference($\Delta P \approx \Delta\pi/2$). Increasing the concentration of the draw solution enhances the performance of the PRO process in terms of water flux and power density by increasing the osmotic driving force, whereas increasing the concentration of the feed solution reduces the water flux and power density. When the draw solution flow rate increases from 2 to 4 L/min, a slight enhancement of power density and water flux was identified.

References

[1] D. I. Kim, J. Kim, and S. Hong, "Changing membrane orientation in pressure retarded osmosis for sustainable power generation with low fouling," *Desalination*, vol. 389, 2016.

[2] K. Touati and M. S. Rahaman, "Viability of pressure-retarded osmosis for harvesting energy from salinity gradients," *Renewable and Sustainable Energy Reviews*, vol. 131, no. February, p. 109999, 2020.

[3] Z. Wang, D. Hou, and S. Lin, "Gross vs . net energy : Towards a rational framework for assessing the practical viability of pressure retarded osmosis," *Journal of Membrane Science*, vol. 503, pp. 132–147, 2016.

[4] F. Helfer, O. Sahin, C. Lemckert, and Y. G. Anissimov, "Salinity Gradient Energy : a New Source of Renewable Energy for," no. February, pp. 3–13, 2013.

[5] A. Janson, D. Dardor, M. Al Maas, J. Minier-Matar, A. Abdel-Wahab, and S. Adham, "Pressure-retarded osmosis for enhanced oil recovery," *Desalination*, vol. 491, no. March, p. 114568, 2020.

[6] N. Y. Yip and M. Elimelech, "Performance limiting effects in power generation from salinity gradients by pressure retarded osmosis," *Environmental Science and Technology*, vol. 45, no. 23, pp. 10273–10282, 2011.

[7] W. Y. Chia *et al.*, "Factors affecting the performance of membrane osmotic processes for bioenergy development," *Energies*, vol. 13, no. 2, 2020.

[8] F. Helfer, C. Lemckert, and Y. G. Anissimov, "Osmotic power with Pressure Retarded Osmosis: Theory, performance and trends - A review," *Journal of Membrane Science*, vol. 453, pp. 337–358, 2014.

[9] K. Gerstandt, K. V. Peinemann, S. E. Skilhagen, T. Thorsen, and T. Holt, "Membrane processes in energy supply for an osmotic power plant," *Desalination*, vol. 224, no. 1–3, pp. 64–70, 2008.

[10] M. Kurihara and H. Takeuchi, "SWRO-PRO system in 'Mega-ton Water System' for energy reduction and low environmental impact," *Water (Switzerland)*, vol. 10, no. 1, pp. 1–15, 2018.

[11] W. A. N. Chunfeng, "Membrane Technology for Osmotic Power," 2016.

[12] M. Yasukawa, D. Shigefuji, M. Shibuya, Y. Ikebe, R. Horie, and M. Higa, "Effect of DS concentration on the PRO performance using a 5-Inch scale cellulose triacetate-based hollow fiber membrane module," *Membranes*, vol. 8, no. 2, 2018.

[13] E. Sivertsen, T. Holt, W. Thelin, and G. Brekke, "Modelling mass transport in hollow fibre membranes used for pressure retarded osmosis," *Journal of Membrane Science*, vol. 417–418, pp. 69–79, 2012.

[14] W. A. Phillip, J. S. Yong, and M. Elimelech, "Reverse draw solute permeation in forward osmosis: Modeling and experiments," *Environmental Science and Technology*, vol. 44, no. 13, pp. 5170–5176, 2010.

[15] Z. L. Cheng and T. S. Chung, "Mass transport of various membrane configurations in pressure retarded osmosis (PRO)," *Journal of Membrane Science*, vol. 537, no. May, pp. 160–176, 2017.

[16] N. Y. Yip *et al.*, "Thin-film composite pressure retarded osmosis membranes for sustainable power generation from salinity gradients," *Environmental Science and Technology*, vol. 45, no. 10, pp. 4360–4369, 2011.

[17] D. Xiao, W. Li, S. Chou, R. Wang, and C. Y. Tang, "A modeling investigation on optimizing the design of forward osmosis hollow fiber modules," *Journal of Membrane Science*, vol. 392–393, pp. 76–87, 2012.

[18] S. Shen, S. E. Kentish, and G. W. Stevens, "Shell-side mass-transfer performance in hollow-fiber membrane contactors," *Solvent Extraction and Ion Exchange*, vol. 28, no. 6, pp. 817–844, 2010.

[19] T. T. Liang and R. L. Long, "Corrections to correlations for shell-side mass-transfer coefficients in the Hollow-Fiber Membrane (HFM) modules," *Industrial and Engineering Chemistry Research*, vol. 44, no. 20, pp. 7835–7843, 2005.

[20] S. Zhang, F. Fu, and T. S. Chung, "Substrate modifications and alcohol treatment on thin film composite membranes for osmotic power," *Chemical Engineering Science*, vol. 87, pp. 40–50, 2013.

[21] Y. Chen, C. Heng, L. Zhang, L. Setiawan, and Q. She, "Module scale-up and performance evaluation of thin fi lm composite hollow fi ber membranes for pressure retarded osmosis," *Journal of Membrane Science*, vol. 548, no. August 2017, pp. 398–407, 2018.

[22] K. L. Lee, R. W. Baker, and H. K. Lonsdale, "Membranes for power generation by pressure-retarded osmosis," *Journal of Membrane Science*, vol. 8, no. 2, pp. 141–171, 1981.

[23] K. Touati, "Energy generation and recovery by Pressure Retarded Osmosis (PRO): Modeling and experiments," 2015.

[24] D. Bharadwaj, T. M. Fyles, and H. Struchtrup, "Multistage Pressure-Retarded Osmosis," *Journal of Non-Equilibrium Thermodynamics*, vol. 41, no. 4, pp. 327–347, 2016.

[25] Q. Ge, M. Ling, and T. S. Chung, "Draw solutions for forward osmosis processes: Developments, challenges, and prospects for the future," *Journal of Membrane Science*, vol. 442, pp. 225–237, 2013.

[26] F. A. Yaseen, A. F. Al-Alawy, and A. Sharif, "Highly-charged EDTA-2Na salt as a novel draw solution in pressure-retarded Osmosis process," *AIP Conference Proceedings*, vol. 2372, no. November, 2021.

[27] Q. She, Y. K. W. Wong, S. Zhao, and C. Y. Tang, "Organic fouling in pressure retarded osmosis: Experiments, mechanisms and implications," *Journal of Membrane Science*, vol. 428, pp. 181–189, 2013.

نمذجة رياضية لوحدة الألياف المجوفة المستخدمة في عملية تناضح الضغط المُثبَّط

[1] فرح عادل ياسين, [2] أحمد فائق العلوي, [3] عادل شريف

[1] شركة النفط الوطنية العراقية, شركة نفط الوسط, بغداد, العراق
[2] قسم الهندسة الكيمياوية, كلية الهندسة, جامعة بغداد, بغداد, العراق
[3] قسم هندسة العمليات والهندسة الكيميائية, جامعة سري، سري، المملكة المتحدة

الخلاصة

يمكن اعتبار عملية تناضح الضغط المُثبَّط (PRO) كإحدى طرق استخدام طاقة التناضح ، وهي تقنية تعتمد على الغشاء. تلعب النمذجة الرياضية دورًا أساسيًا في تطوير وتحسين أنظمة PRO لتوليد الطاقة. في هذا البحث ، تم تطوير نموذج رياضي لوحدة الألياف المجوفة للتنبؤ بكثافة الطاقة و تَدَفُّق الماء نظريًا. تم استخدام محلول كلوريد الصوديوم كمحلول تغذية ومحلول سحب. تم استخدام عوامل تشغيل مختلفة, تركيز محلول السحب (1 و 2 مولاري) ، ومعدل تدفق محلول السحب (2 ، 3 ، و 4 لتر / دقيقة)، فرق الضغط الهيدروليكي المطبق (0–90 بار) لتقييم أداء عملية PRO لوحدة الألياف المجوفة. تم دراسة تأثير هذه المتغيرات التشغيلية على تدفق المياه وكثافة الطاقة النظرية. وفقًا للنتائج النظرية ، زاد تدفق الماء المتخلل وكثافة الطاقة مع زيادة تركيز محلول السحب ومعدل تدفق محلول السحب. بينما انخفض تدفق الماء المتخلل وكثافة الطاقة مع زيادة تركيز محلول التغذية. بزيادة الضغط الهيدروليكي المطبق على محلول السحب ، انخفض تدفق الماء وزادت كثافة الطاقة الناتجة. كانت كثافة الطاقة القصوى وتدفق الماء المتخلل حوالي 16.414 واط/م^2 و 11.818 لترام^2.ساعة على التوالي عند استخدام محلول سحب 2 مولاري كلوريد الصوديوم ، والذي يحدث عند ضغط هيدروليكي مطبق قدره 50 بار.

الكلمات الدالة: النموذج الرياضي ، طاقة التناضح ، غشاء ليفي مجوف ، تناضح الضغط المُثبَّط.